ACCEPTED MANUSCRIPT

Atomic force microscopy analysis of surface topography of pure thin aluminum films

Atomic force microscopy analysis of surface topography of pure thin aluminium films

F.M. Mwema[1], O.P. Oladijo[2,1], T.S. Sathiaraj[2], E.T. Akinlabi[1]

[1]Department of Mechanical Engineering Science, FEBE, University of Johannesburg, Auckland Park, Kingsway Campus, 524, Auckland Park 2006, Johannesburg, South Africa
[2]Botswana International University of Science and Technology, Private Bag 16, Palapye, Botswana

Abstract

Pure aluminium thin films were deposited on stainless and mild steel substrates through rf magnetron sputtering at rf powers of 150 and 200 W. Surface analysis of the films was undertaken using atomic force microscopy. The surface structure evolution, roughness and distribution were examined and discussed. Power spectral density, skewness and Kurtosis parameters were used to explain the nature and distribution of the surface structures on the thin aluminium films as reported from the line profile analyses. The result shows that the morphologies of the surface structures of Al films vary with power and substrate type. The coatings exhibit the higher roughness at 200 W. There is strong links that exist between AFM observations and SEM. This implies that AFM can be considerably used to study the microstructural evolution of Al thin films during magnetron sputtering.

Keywords: Atomic Force Microscopy, Magnetron sputtering, Power Spectral Density, Surface roughness, Thin aluminium films

1. Introduction

Thin aluminium films are widely used as protective coatings to improve surface properties of substrates. This is because they offer combination of excellent properties such as resistance to oxidation, corrosion and wear to metal substrates [1]. They are widely utilized for corrosion protection on low carbon steels [2–6], aluminium-magnesium alloys [7, 8] and stainless steel 304 [9]. They are also used for diffusive intermetallic coating of titanium alloys [10].

Physical methods of preparing thin films are preferred over chemical techniques because they provide high substrate-film adhesion and quality thin films [11]. A rich literature therefore exists on studies of Al thin films deposited on different substrates through thermal [1, 3, 5, 12, 13] and physical vapor deposition [14] methods. However it has been reported that Al thin films prepared

through thermal methods have higher density of porosity and defects, which limit their applications as surface protectors for substrates [4, 10]. As such, physical vapor deposition (PVD) methods such as magnetron sputtering are preferred in preparing Al thin films.

A detailed look into the existing literature shows that most works have reported on magnetron deposition of Al thin films on non-metals [15], with limited studies on Al thin films on metallic substrates. The properties of Al thin films depend on the PVD deposition conditions and parameters. The effects of substrate temperature [16], deposition gas (argon) pressure [16, 17], deposition rates, deposition power [16], bias voltage in magnetron sputtering [17], etc. on the properties of Al thin films have been reported. Studies [18–20] reported on the effect of film thickness on the structural properties of Al thin films sputtered on different substrates. Structural zone models (SZM) have been used to describe the effect of depositions conditions to the structural evolution during thin film growth [21]. According to SZM, there are three regions, namely, Zone I, Zone T and II, used to explain the evolution of microstructure in thin films. The evolution of microstructure in this model is explained in terms of adatom mobility. Zone I occur when the deposition parameters such as temperature, rate, etc. lead to low adatom mobility. In this case, microstructure of thin films consists of fine fiber, porous or even amorphous texture. There are small and more equiaxed grains. In transition zone, T, there is higher diffusion of adatoms, leading to formation of coarser structures. There is competitive grain growth and a preferred crystallographic orientation with respect to the film thickness are likely to occur. In zone II, there is bulk mobility of adatoms, grain growth and recrystallization which causes formation of coarser/columnar structures on the films.

Atomic force microscopy (AFM) is a powerful profilometry technique used in studying the surface topography of thin films. It gives quantitative information about the surfaces and surface structures [22]. It also studies the surface microstructure of thin films [23, 24]. Through AFM imaging, morphological information of the surfaces of thin films can be expressed in terms of roughness, maximal and mean heights of the structures[25–27]. AFM also studies the grain size and distribution in thin films [28]. Additionally, AFM images can be examined through fractal geometry techniques such as power spectral density (PSD) functions to describe various complex surface morphologies and their effects on the surface properties of the film [29]. The surface properties significantly influence strength and corrosion performance of Al thin films and it is

therefore necessary to study them. The present work reports on the topographical properties of Al thin films prepared through r.f magnetron sputtering using AFM. Al thin films were deposited on stainless and mild steel substrates at rf powers of 150 W and 200 W.

2. **Experimental Procedure**

Pure Al coatings were prepared by rf magnetron sputtering. A solid pure Al target of 99.9% purity, with diameters 75 mm and thickness 3 mm were used. Two different metal substrates namely mild steel and stainless-steel plates of size 75 x 25 x 3 mm were used. The substrates were initially cleaned with acetone, isopropanol and finally with deionized water for 15 mins respectively. Prior deposition the substrate was held onto a non-rotating work holder directly above Al target to maximize the material absorption by the substrate. The distance between the target and substrate was kept at 13 cm. The sputtering apparatus was first evacuated to a base pressure of 1.13 x 10-5 mbar, after which the Al thin films were deposited at room temperature. The flow rate of argon was kept constant at 12 sccm and the working pressure maintained at about 1.20 x 10-2 mbar. Two different substrates of each metal were sputtered at 150 W and 200 W for 2 hours.

The coated samples were then cut into 10 x 10 mm sizes for SEM, XRD and AFM analyses. SEM and XRD were undertaken to observe the morphology and crystallinity of the Al thin films respectively. AFM was conducted on Veeco Dimension 3100 AFM facility. The imaging was conducted in tapping mode with a cantilever of spring constant of 2.8 N/m with a resonance frequency of 75 kHz. The images were taken at a scan size of 3x3 μm at integral and proportional gains of ranges of 0.4-0.8 and 0.6-1.0 respectively. The optimal set point for the images ranged between 0.899 and 1.120. Five AFM images were taken at different sections of the sample surface at the same gain conditions, scan rate and size. The image analyses were performed in Nanoscope V530r3sr3 and Matlab® software. Roughness from AFM imaging was expressed in terms of mean heights (Ra) and root mean square (R_{rms}) computed using equations 1 and 2 respectively [30].

$$R_a = \frac{1}{L_x L_y} \sum_{j=1}^{L_y} \sum_{i=1}^{L_x} |Z_{ij} - \mu| \qquad (1)$$

$$R_{rms} = \sqrt{\frac{1}{L_x L_y} \sum_{j=1}^{L_y} \sum_{i=1}^{L_x} (Z_{ij} - \mu)^2} \qquad (2)$$

Where;

μ is the mean given as $\mu = \frac{1}{L_x L_y}\sum_{j=1}^{L_y}\sum_{i=1}^{L_x} Z_{ij}$

Lx, Ly represents the data sample size/sampling length

Zij is the profile height function/ source discrete function on the XY plane of the sampling surface

To characterize the symmetry of distribution of the structures of surfaces, surface skewness [30], R_{sk}, was used and calculated from AFM images as follows.

$$R_{sk} = \frac{1}{L_x L_y R_{rms}^{3}}\sum_{j=1}^{L_y}\sum_{i=1}^{L_x}(Z_{ij}-\mu)^{3} \qquad (3)$$

For symmetric distributions, nonzero values of R_{sk} are recorded. Also, when the positive values are recorded, it means that the surface is dominated by peaks whereas when the values are negative, the surface is dominated by valleys. To measure spikiness of height distribution of the surface, coefficient of kurtosis, R_{ka}, was calculated as follows [30].

$$R_{ka} = \frac{1}{L_x L_y R_{rms}^{4}}\sum_{j=1}^{L_y}\sum_{i=1}^{L_x}(Z_{ij}-\mu)^{4} - 3 \qquad (1)$$

If $R_{ka}=3$, the surface has Gaussian distribution, if $R_{ka} > 3$, then the surface is spiky and when $R_{ka} < 3$, the surface is considered bumpy.

Although the above statistical methods are simple and reliable, they do not account for lateral distribution of topographic features and do not show the distinction between peaks and valleys [29, 31]. As such, power spectral density (PSD) of surface topography is more descriptive and uses Fourier transform (FT) to decompose the surface profile into spatial wavelengths and allows comparison of roughness measurement in frequency domain of the image. PSD basically transforms AFM images into complex frequency domain through Fast Fourier Transform (FFT). A 2-dimensional PSD (S_2) of a surface described by its topography function $z(x,y)$ is written as follows [31]

$$S_2(f_x, f_y) = \lim_{L\to\infty}\frac{1}{L^2}\left\{\int_{-\frac{1}{2}L}^{\frac{1}{2}L} dx \int_{-\frac{1}{2}L}^{\frac{1}{2}L} dy . z(x,y). exp[2\pi j(xf_x + yf_y)]\right\}^2$$

(2)

Where

L is the scan length assumed to be equal in x and y directions.

f_x, f_y spatial frequencies (inverse of wavelengths) for x and y directions respectively

j is the complex part

z(x,y) is the height/profile surface function

The equation above is not exactly FT of z(x,y) function, we need to work in finite N of values assumed equidistantly placed in x,y directions at distances $\Delta x, \Delta y = \frac{L}{N}$. The 2D PSD is then written as shown in Equation 6 [31].

$$S_2(f_x, f_y) = L^2 \left[\frac{1}{N^2} \sum_{n=0}^{N} \sum_{m=0}^{N} z(x_m, y_n) exp(2\pi j. x_m f_x) exp(2\pi j. y_n. f_n)\right]^2$$

(3)

Where $x_m = m.\frac{L}{N}$, $y_n = n.\frac{L}{N}$ and f_x, f_y take discrete range of values as $f_x, f_y = \frac{1}{L}, \frac{2}{L}, \dots \dots \dots . \frac{N}{2L}$

In this work, PSD functions were calculated according to equations 5 and 6 on AFM images. The PSD functions were fitted into two models. At low spatial frequencies, the functions were fitted into K-model (also known as ABC model) whereas at higher spatial frequencies, the PSD functions were fitted in inverse power law (or fractal model). The K-model is expressed by equation 7 [29].

$$PSD = \frac{A}{(1+B^2 f^2)^{C+\frac{1}{2}}}$$

(4)

This model describes the random distribution of roughness of surfaces of large length scales. It gives a PSD function with a knee, which is described by B, constant PSD region at very low values of frequency, f, determined by A and at very high values of frequency, the surface is fractal determined by C. A is related to very low frequency component of roughness and B is the correlation length related to grain size [29]. The equivalent roughness (σ) and correlation length (τ) according to the K-model are given as $\sigma = \frac{2\pi A}{B^2(C-1)}$ and $\tau = \frac{(C-1)^2 B^2}{2\pi^2 C}$ respectively.

The inverse power law (fractal model) is expressed in equation 8 [32]. From the equation, K is the spectral length and γ is the gradient for the log-log PSD vs spatial frequency plot.

$$PSD = \frac{K}{f^\gamma}$$

(5)

From equation 8, the fractal dimension, D can be determined according to the following criteria.

When $0 \le |\gamma| < 1$, then $D = 2$ or $3 < |\gamma|$, then $D = 1$; otherwise, $D = \frac{1}{2}(8 - \gamma)$. The roughness scaling factor, H, known as the Hurst exponent can also be related to the fractal dimension as $D = 3 - H$.

3. Results and discussion
3.1.   Stainless Steel Substrates

Figure 1 shows the AFM images of Al thin films deposited on stainless steel substrates at 150 W and 200 W. The images reveal well defined and spherical grains for both powers. At 150 W (Figure 1a), the surface topography was characterized by small-clustered, large and irregularly-packed

structures (heterogenous). At 200 W, small, regular and closely-packed structures were observed. This is in agreement with the characteristics of zone T in the structure zone model [21]. However, there were surface holes, trenches and ditches of arbitrary shapes observed at 200 W (Figure 1d). On the righthand side of the 2D AFM images (Figure 1a and 1c), there are intensity strips shown. These strips are used to estimate the depth and height along the z-axis of the images if optimal scale setting of the scope trace is achieved. Interpretation of these strips at the two powers, reveals that the thickness of Al thin film during rf magnetron sputtering increased from 150 to 200 W. Table 1 shows the calculated root mean square (R_{rms}), height (R_a), skewness (R_{sk}) and kurtosis (R_{ka}) values for all the analysed samples. It can be deduced that the roughness of Al thin films deposited on mild steel substrate increased with power of deposition. This is in agreement with the literature [33]. That further implies that the roughness increased with the film thickness. Thicker films have been shown to have higher roughness due to grain growth and larger grains [18]. However, in this study, the increase in roughness can be attributed to arbitrary holes, trenches, ditches and spraying parameters on the surface. Similar explanation has been provided for thermally evaporated Al thin films on quartz substrates [34].

To study the heights and widths of structures of the films, five AFM topographic 2D images were analysed as shown in Figure 2. For each image, three cross sections (1,2,3) were measured and a profile line diagram of depth (z-axis) against the surface along the x-axis was generated. The averages values for height (H) and widths (W) were calculated and reported for each cross section. The overall mean heights (H_{av}) and widths (W_{av}) and their corresponding maximum (H_{max} and W_{max}) values were recorded (Table 1). The values of skewness and kurtosis are 0.1976±0.002 and 1.153 respectively at 150 W. This indicates that the surface features are symmetrical, dominated by peaks and bumpy [30]. This observation is in line with the 3D AFM height image indicated by the white arrows and clusters (Figure 1b). This suggested the reason for spiral or wavy appearance of line profiles for thin films deposited at 150 W (Figure 2). The films deposited at 200 W revealed serrated line profiles across their surfaces (Figure 3). This result agrees with the values of skewness and kurtosis in Table 1, which clearly shows the surface is spiky and dominated by valleys. A 3D AFM phase image (not shown) clearly revealed spikes and valleys on samples prepared at 200 W. The width W in this case is used to illustrate the size of the surface structures such as grains. The smaller the W values the smaller particles and closer the particles to each other. The values of W are small at 200W as compared to 150 W. This is the reason for serrated line profiles in Figure 3. However, it is thought that, the presence of defects as holes, trenches and ditches is the reason for steep deeps (indicated as 1 in Figure 3) of the line profiles and hence the reason for increase in roughness (Figure 1d). The smaller values of W at 200 W indicates densification and packing of relatively smaller structures, although with height deviations. As shown by line profiles, this close packing makes the surface to appear laterally homogenous but with valleys and spikes, making the surface appear serrated. These observations can be understood by considering the nucleation and coalescence processes during film formation [21, 34].

Figures 4(a) and 4(b) show the power spectral density profiles (logarithmic) of AFM images at 150 W and 200 W respectively. Generally, the experimental profiles exhibit a PSD constant region at low spatial frequency corresponding to white noise and a steep decrease in PSD at higher spatial frequencies corresponding to highly correlated region. At 200 W, the white noise region is larger than at 150 W. This indicates some extend of homogenous lateral distribution of roughness of surface structures at 200 W. This observation correlates well to the serrated line profiles with occasional 'ditches' indicated as 1 in Figure 3. Furthermore, comparing the logarithmic X-scales for both figures, it emerges that at 200 W, the scale range was higher than that of 150 W. This is an indication that images at 200 W have smaller spatial wavelengths, hence there is uniform distribution of small particles over the surface of the image. It therefore means that at 200 W, the smaller and closely packed particles do not create large and uneven distribution throughout the matrix. It is therefore suggested that the lateral distribution of particles at 200 W is homogenous; and the reason for increased roughness is due to the steep deeps/trenches (Figure 3). The PSD functions are both dominated by the power law, which indicates that the surfaces are generally rough. The high roughness observed on these surfaces was the reason for choice of very small scan size (3x3 um) during AFM imaging. At scan sizes beyond 5x5 um, the AFM scope (not shown) was characterized by very high noise and frequent retraction. Table 2 shows slight increase in power law exponent, γ and decrease in PSD amplitude, K from 150 W to 200 W. This indicates higher surface roughness at 200 W and increase in height features within the lateral range. Additionally, increase in power law at 200 W indicates growth of features at different wavelength and different rates of growth [35]. The B parameter in the K-model describes the sizes of the surface structures [36]. At 200 W the value of B (grain size) is smaller than at 150 W (Table 2). This agrees with the line profile analysis (Figures 2 and 3). There are considerable differences between A and C parameters (Table 2) for both powers; which indicates considerable differences in lateral distribution in roughness and surface structures [37]. The fractal dimensions (D) are computed as 2.87 and 2.83 at 150 W and 200 W respectively for stainless steel substrate (Table 2). The Hurst components (H) are 0.13 and 0.17 at 150 W and 200 W respectively for stainless steel substrates. Generally, when H is between 0 and 0.5 it means the surface contains continuous alternating height features indicating uniform distribution while at range 0.5-1.0 indicates spatial series with positive autocorrelation [29]. This means that there are sharp changes in surface features hence inhomogeneous distribution of the surface features [38, 39].

3.2.   Mild Steel Substrates

Figure 5 shows 2D and 3D AFM images of Al thin films deposited at 150 W and 200 W. It can visually be seen that at 150 W, the surface consists of small, close-packed, globular and nearly uniform structures while the surface structures appear larger and clustered at 200 W. This indicates that at higher power, there is growth of surface structures and hence densification of large particles on the surface. The structures at 200 W appear elongated and highly interconnected. As shown in Table 1, higher roughness is recorded on thin films deposited at 200 W. This can be attributed to increase in size of surface structures as further confirmed by W in Table 1 [34]. It can also be seen that standard deviation for average heights of structures (H_{av}) is higher at 200 W, indicating presence of extremes on the surface structures. The growth of surface structures with rf power can be explained by considering that increase in rf power leads to increase in deposition rate [40] and hence diffusion of adatoms, nucleation and coalescence [34]. At lower rf power, the diffusion of Al atoms and formation of Al clusters is insignificant whereas at higher power, there is higher density of Al atoms arriving onto the substrate surface and hence larger number of nuclei forms leading to larger grains. Figures 6 and 7 show the line profiles across the selected three sections of the surface. The morphology of the films (at 150 W) consists of valleys with many but less pronounced peaks making the line profiles appear nearly serrated (Figure 6). The serrations imply that the surface morphologies are closely packed. At 200 W, the valleys are clearly separated by wide deeps, indicating long and large surface structures (Figure 7). These observations agree with skewness and kurtosis values in Table 1.

Figures 8(a) and 8(b) show the log PSD versus log spatial frequency plots for Al thin films deposited on mild steel substrates at 150 and 200 W respectively. The modelling parameters for K- and fractal models are summarised in Table 2. There is a clearer white noise region in Figure 8(a) than in Figure 8(b), indicating higher homogeneity on surfaces deposited at 150 W. Generally, based on the Hurst exponents in Table 2, the surface structures are homogenously laterally distributed. It can also be noted that for the two powers, PSD amplitude, K and power exponent γ in the fractal model are different, which means that growth rate of surface structures (such as grains) occur at different rates at different powers. Unlike, in stainless steel substrates, the PSD amplitude (K) increased and it shows no correlation with the roughness trend. The results of the K-model show that grain size parameter B is higher at 200 W, indicating grain growth. This is

consisted with the morphological quantification of the line profile analysis. It is also shown that the roughness components (A) at low frequency for the two powers are nearly equal (Table 2). This can be confirmed by the R_{rms} and Ra results in Table 1, which generally shows very close values for the two parameters for both powers. The fractal parameter, C for both powers are also very close; indicating that the lateral distribution of roughness on these surfaces is also similar.

From the preceding discussion, there are differences in topographical characteristics of the Al films on the stainless steel and mild steel substrates. At both rf powers, the H and W values were higher in mild steel substrates than in stainless steel substrates, which implies that substrate type influences the surface roughness and structures of the thin film coating [41,42]. The size of surface structures (W) increased with rf power in mild steel substrate whereas decreased in stainless steel structures. Additionally, the roughness values and their standard deviations were higher in stainless steel substrate than the mild steel. The AFM images in coated mild steel substrates revealed grainy surfaces characterised by nearly spherical shapes of uniform sizes and it is the suggested reason for the lower roughness and standard deviations of roughness values in mild steel substrates.

3.3.   Coating Microstructure

To support the AFM microstructural observations, the SEM images and XRD results at the top surface of the Al thin films deposited at 150 W and 200 W for the two substrates were investigated and shown in Figures 9, 10 and 11. A similar approach has been used in literature to analyze thin films [43] since SEM can show other important aspects of sputtering such hillock formation [44]. The SEM images show that there were no significant observable differences on stainless steel substrates at 150 W and 200 W (Figure 9a and 9b). The structure consisted of small, shiny, dark regions and defined grains and boundaries. The boundaries were observed as 'interconnected paths' throughout the structure. At higher magnifications (Inset), the shiny regions were observed to be Al structure seen as "impinges" on stainless steel structure at 150 W. This can be related to the AFM images in Figure 1. For both powers, the dark regions were observed as pores resulting from Al deposition. Although the microstructure appears homogenous, at high magnifications, the clusters of Al structures make the surface appear heterogenous. This suggests the differences in roughness and surface profiles measured by AFM. The EDS (not shown) revealed that the dark regions indicated as P on the SEM image have high concentration of oxides.

On the mild steel substrate, the Al structure clearly appeared as 'splats' morphologies at 200 W (Figures 9c and 9d). At 150 W, the SEM images revealed shiny and dark regions, which were identified as areas of high Al and O elements by EDS. At 200 W, the microstructure consisted of long plates of Al and shiny bubble regions as seen in Figure 9d. The bubble region indicated high concentration of O through EDS with no Al elements observed. These observations confirm the AFM observation in Figure 5, which shows increase in size of surface structures. The higher roughness values recorded at 200 W can be attributed to the larger, interconnected structures on the surface. The surface roughness can also be attributed to the porous regions indicated by letter P on the SEM images.

Figures 10 and 11 shows the X-ray diffraction spectra of the magnetron sputtering coating surface using Cu-kα radiation. All the coating had a broad peak at 2θ≈15°. The XRD results of the coated 316L stainless steel substrate showed Chromium-Nickel and Aluminium phase on both sample rf power at 150 W and 200 W respectively (Figure 10). There was no new phase formed on increasing the rf power from 150 W to 200 W, although the Cr-Ni and Al peaks became clearer and intensity higher. This could be attributed to the reduction in stress. In addition, high diffraction background was observed on both XRD spectra because of the strain effects on the coating. The XRD results on the coated mild steel substrate (Figure 11) reveal the presence of Al-Fe, Al and Fe on both coating rf power at 150 W and 200 W respectively. It is thought that the occurrence of Fe on the sputtering surface suggested that diffusion occur between the target atoms (i.e. Al) and Fe in the parent material. This observation confirms the inference of AFM results on the growth of surface structures. No new phases were observed except the presence of high diffraction background. This could be due to strain effect.

4. Conclusions

Al thin films deposited on stainless and mild steel substrates through rf magnetron sputtering were characterised through AFM. Higher roughness was reported for higher rf power for both steel substrates. Besides formation of interconnected structures at higher rf power, increase in roughness can also be attributed to the holes, trenches and ditches observed on the AFM images. Line profile analyses on AFM images were used to study the morphology of structures on the films. It was shown that it is possible to sufficiently describe the surface of the thin films with this technique

since the profiles correlated well with the skewness and kurtosis values. With line profile analyses, the surfaces were described as either wavy, bumpy or serrated. K- and power law models were used to analyse the PSD of the AFM micrographs. For both rf powers, the PSD profiles were shown to have to significant regions, namely the white noise and highly correlated regions as reported in literature [45]. The PSD modelling correlated well with roughness and line profile results. SEM results showed different morphologies of the Al thin films on different substrates. In stainless steel substrates, the Al films appeared as impinges whereas in mild steel substrates they appeared as splats and highly interconnected structures. XRD results showed that highly crystalline Al films are formed when prepared through rf magnetron sputtering on steel substrates at 150 W and 200 W.
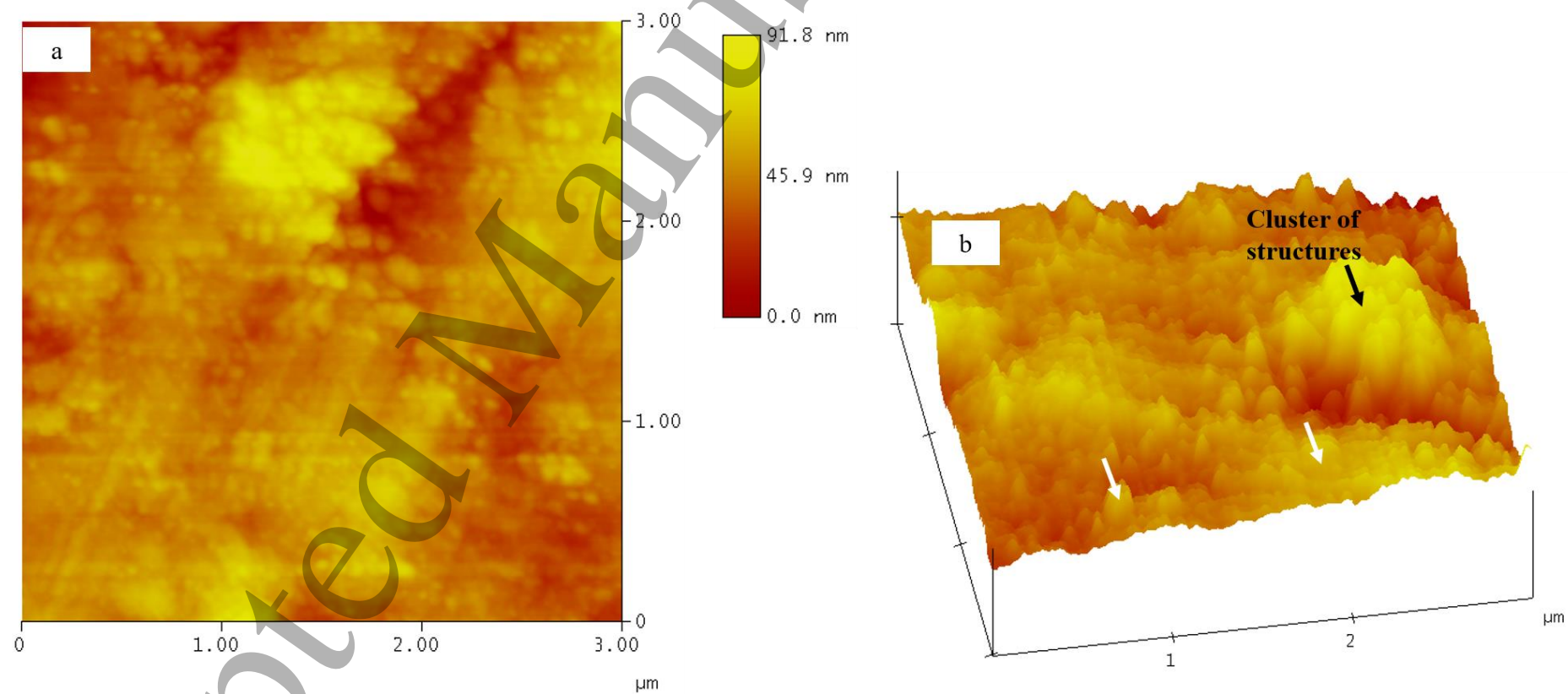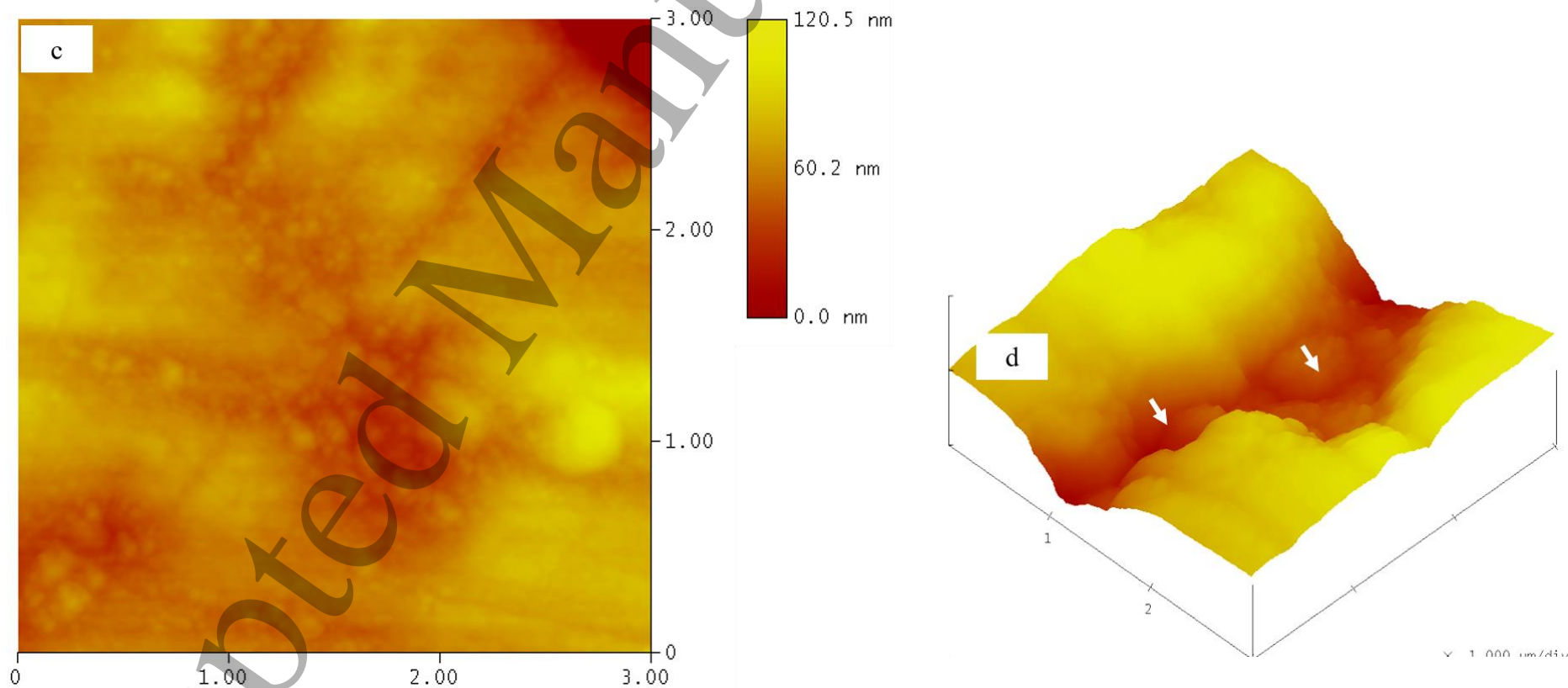
Figure 1. 2D height AFM images for Al thin film surfaces deposited through rf magnetron on stainless steel substrates at (a) 150 W and (c) 200 W rf powers. Figures (b) and (d) shows the corresponding 3D images respectively. The white arrows in Figure 1(b) shows the peaks and cluster of structures responsible for bumpy surfaces (Rka) whereas the white arrows in Figure 1(d) shows the 'ditches' which can be interpreted as defects on the surface of the films
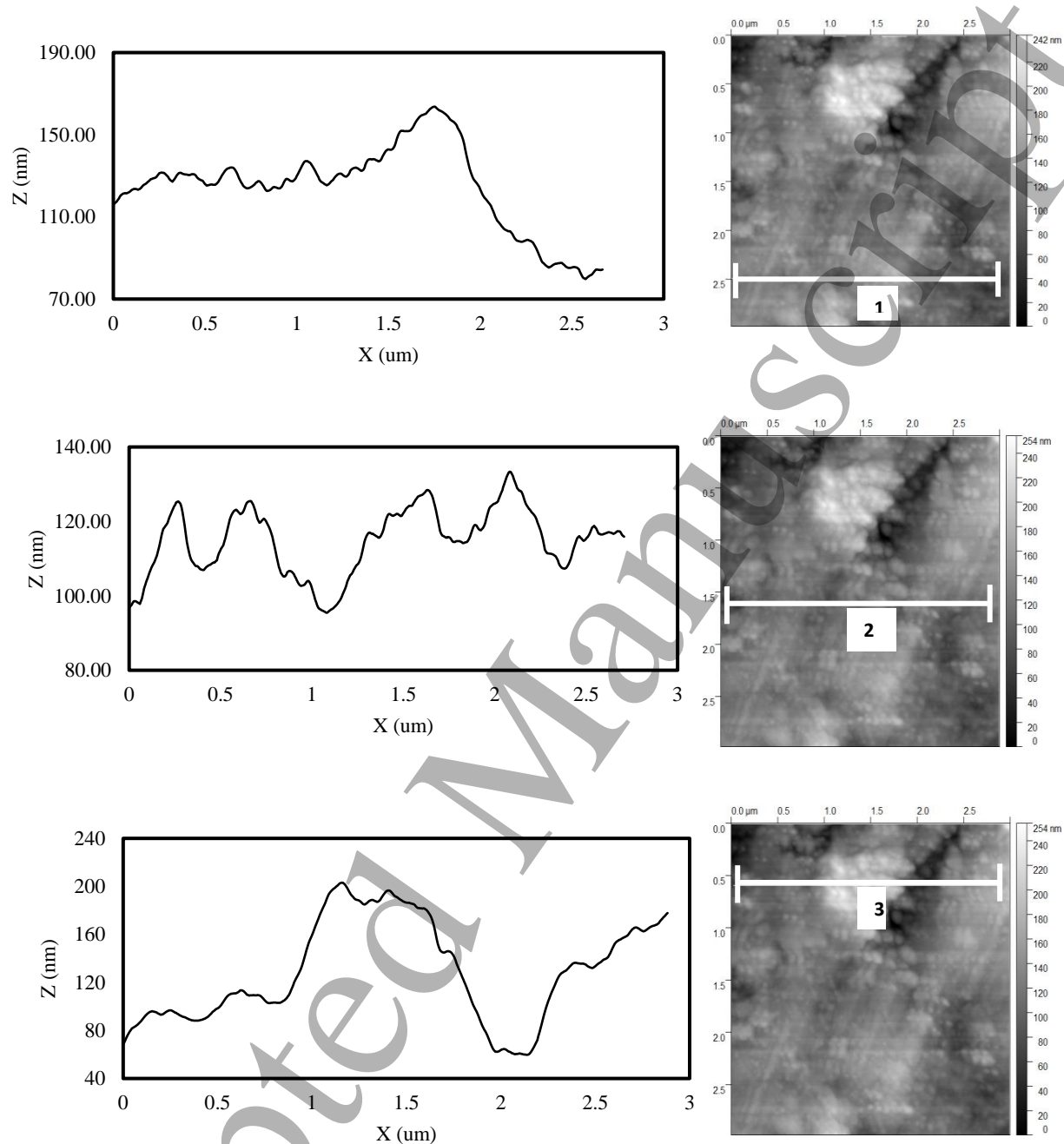
Figure 2. Illustrating the morphological measurements in this work for stainless steel substrates coated at 150 W. Surface profiles were taken at three different sections (1,2,3) of the AFM topographic image. The maximum profile (grain) heights (Hmax), maximum grain widths (Wmax), average heights (Hav) and widths (Wav) along the three sections were determined. In section, 3, due to cluster of small grains seen in Figure 1b higher values of heights and widths were recorded.
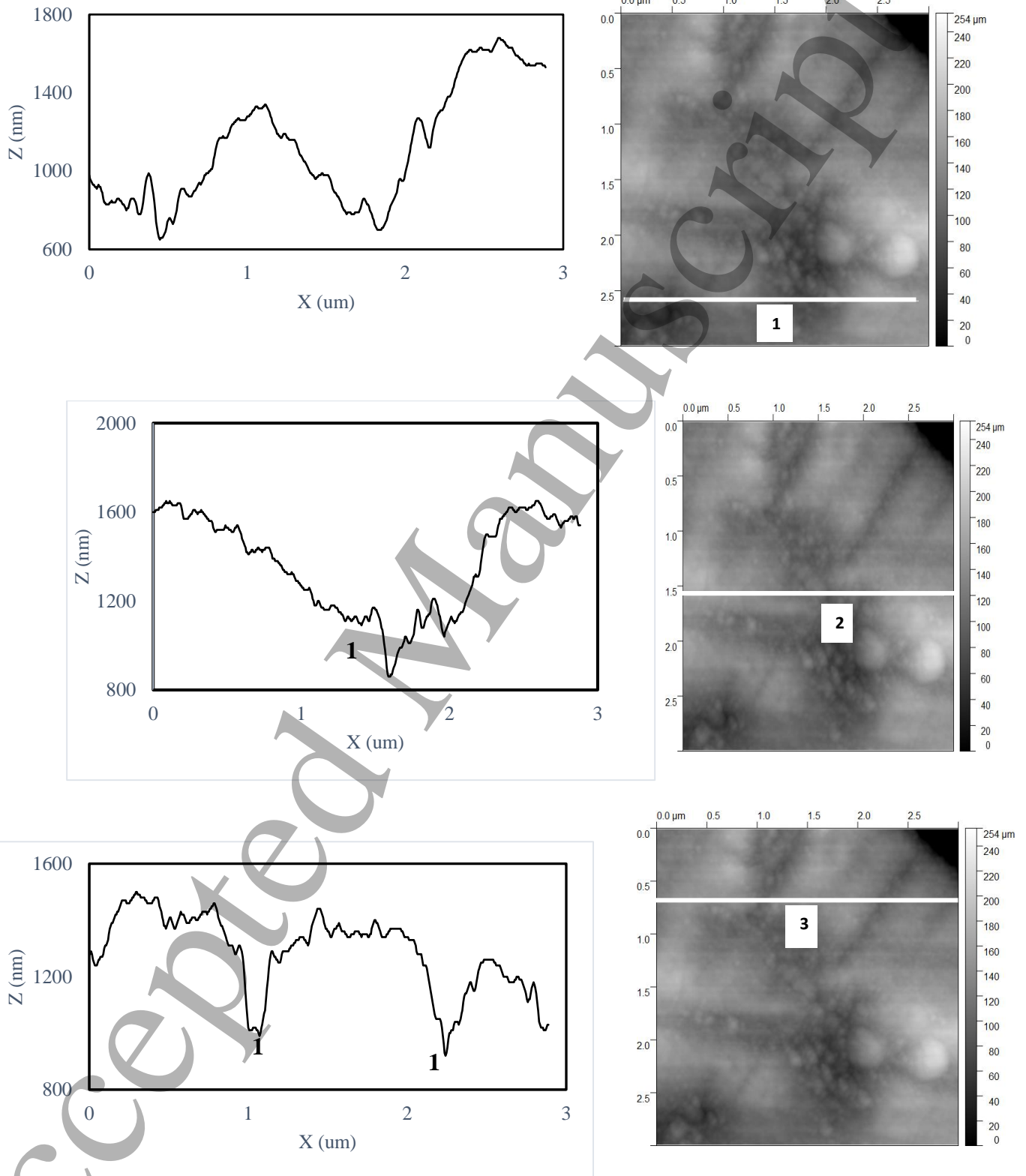
Figure 3. Line profile analysis for Al thin films' surfaces deposited on stainless steel substrates at 200 W.
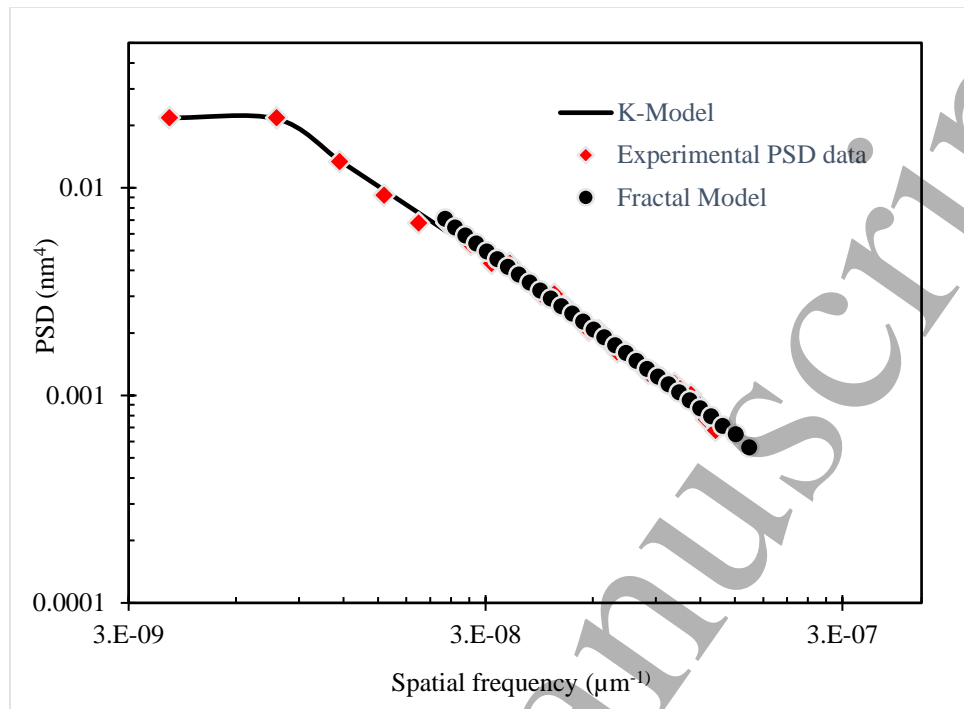
(a)
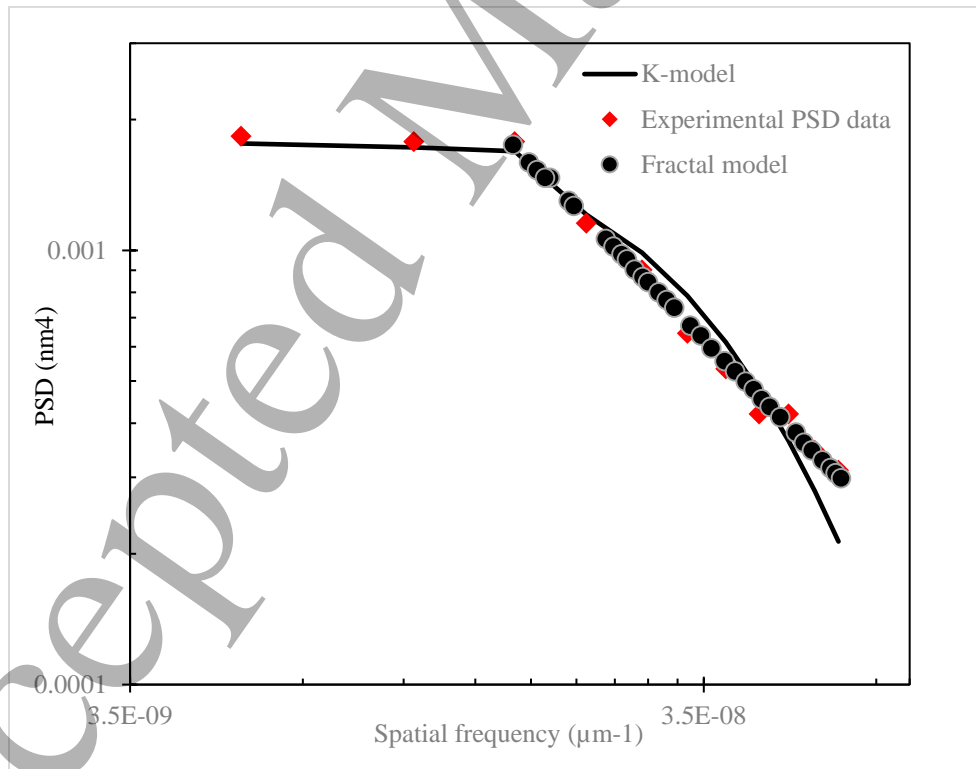
(b)

Figure 4. PSD profiles displayed on double log scale as functions of spatial frequency for Al thin films deposited on stainless steel substrates at (a) 150 W and (b) 200 W. The K-model fits the experimental PSD data at low frequencies whereas the fractal model fits the data at higher spatial frequencies. The model parameters are presented in Table 2.
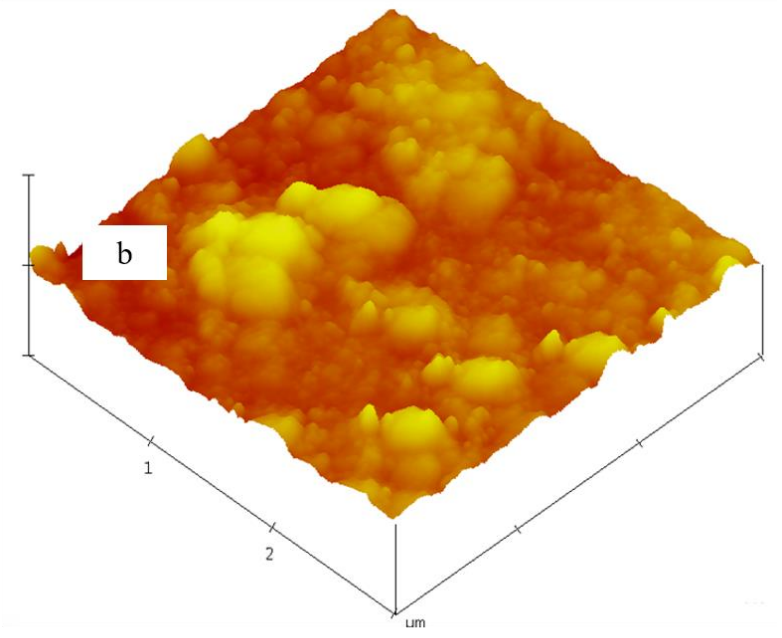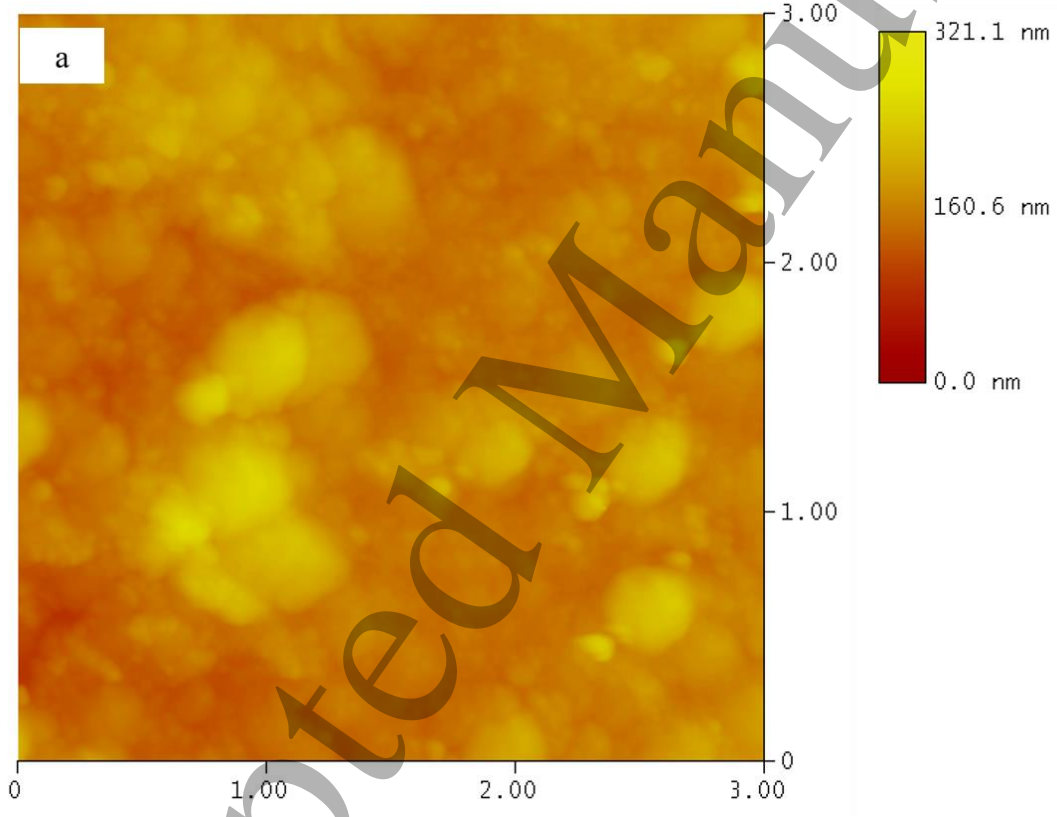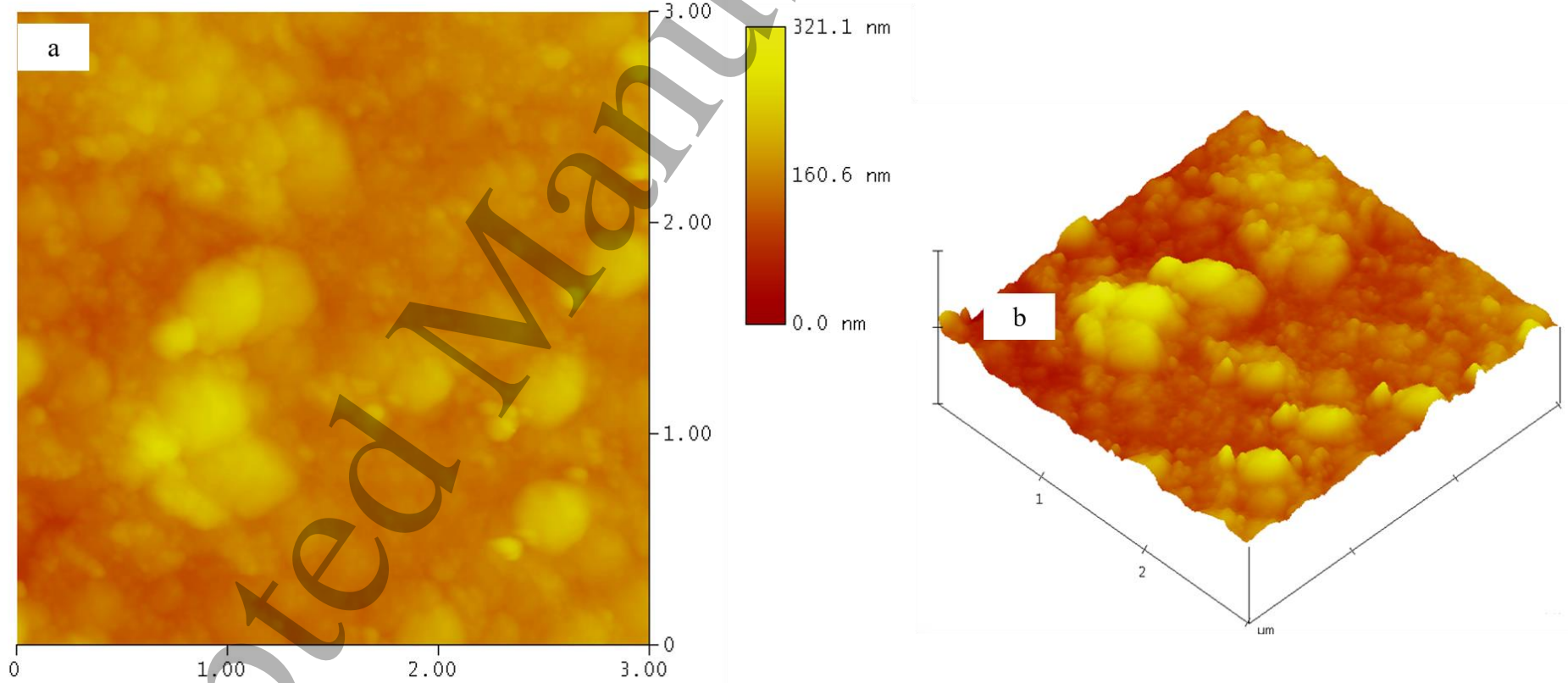
Figure 5. 2D height AFM images for Al thin film surfaces deposited through rf magnetron on Mild steel substrates at (a) 150 W and (c) 200 W rf powers. Figures (b) and (d) shows the corresponding 3D images respectively.
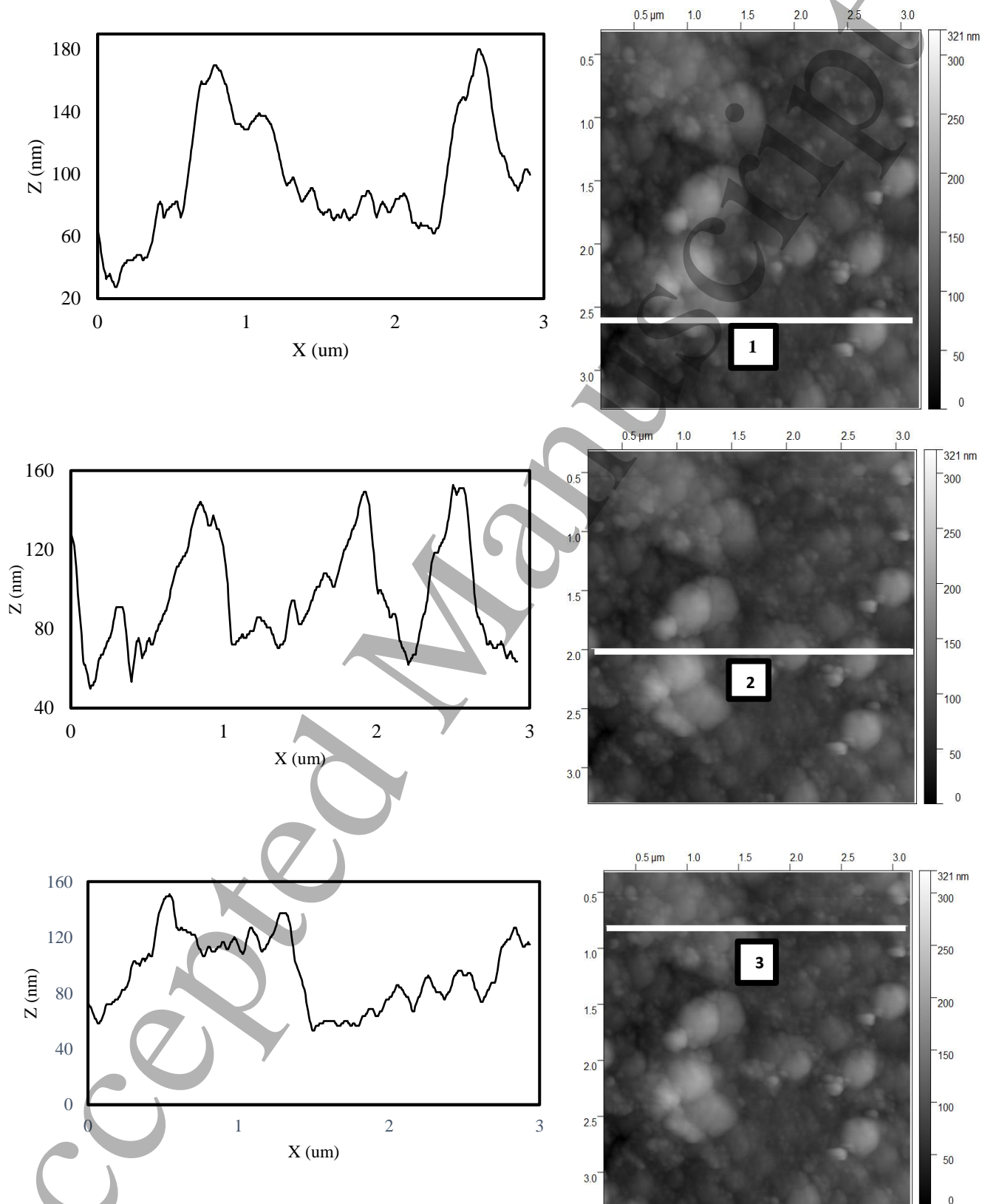
Figure 6. Line profile analysis for the surfaces of Al thin films deposited on mild steel substrates at 150 W
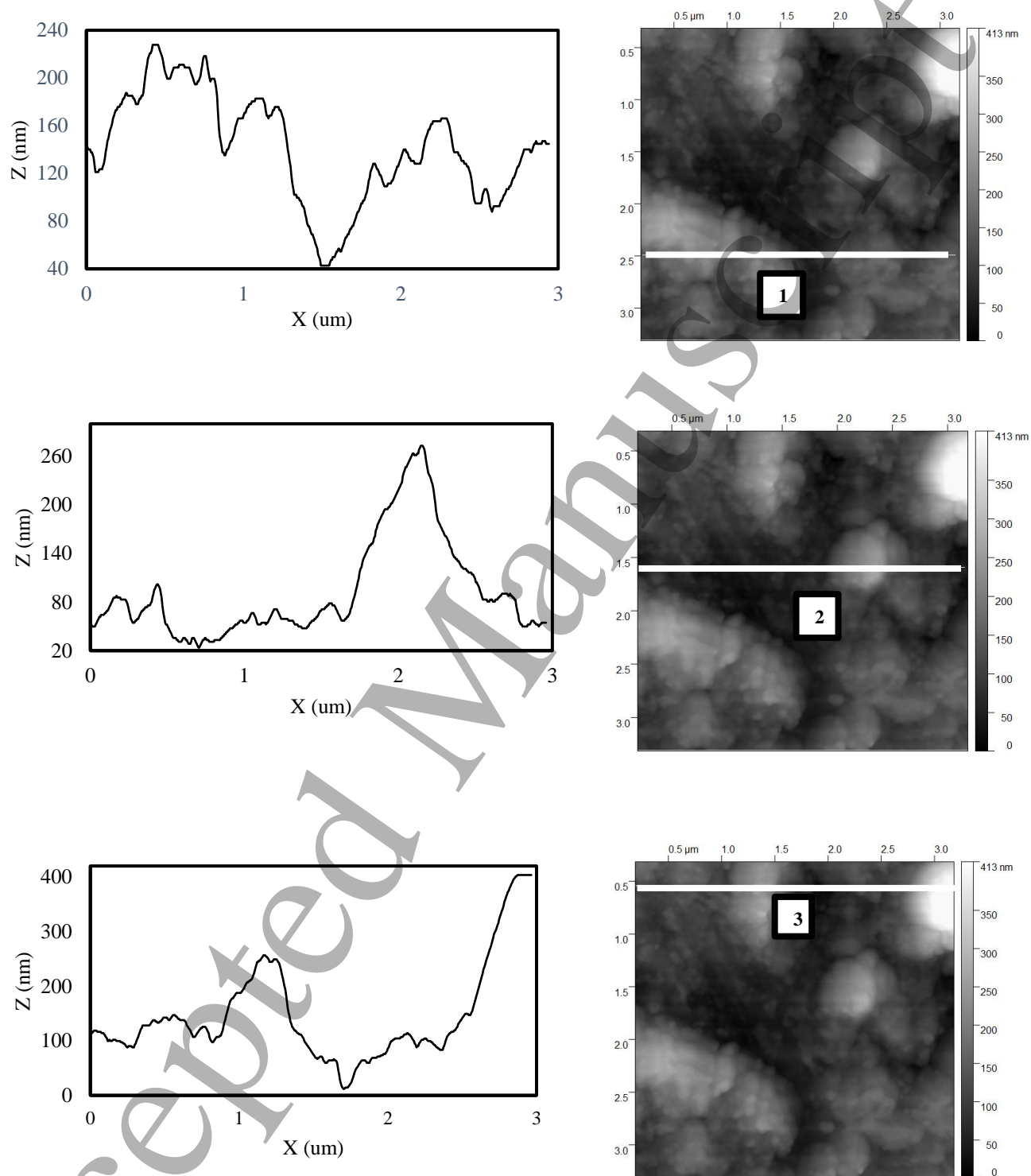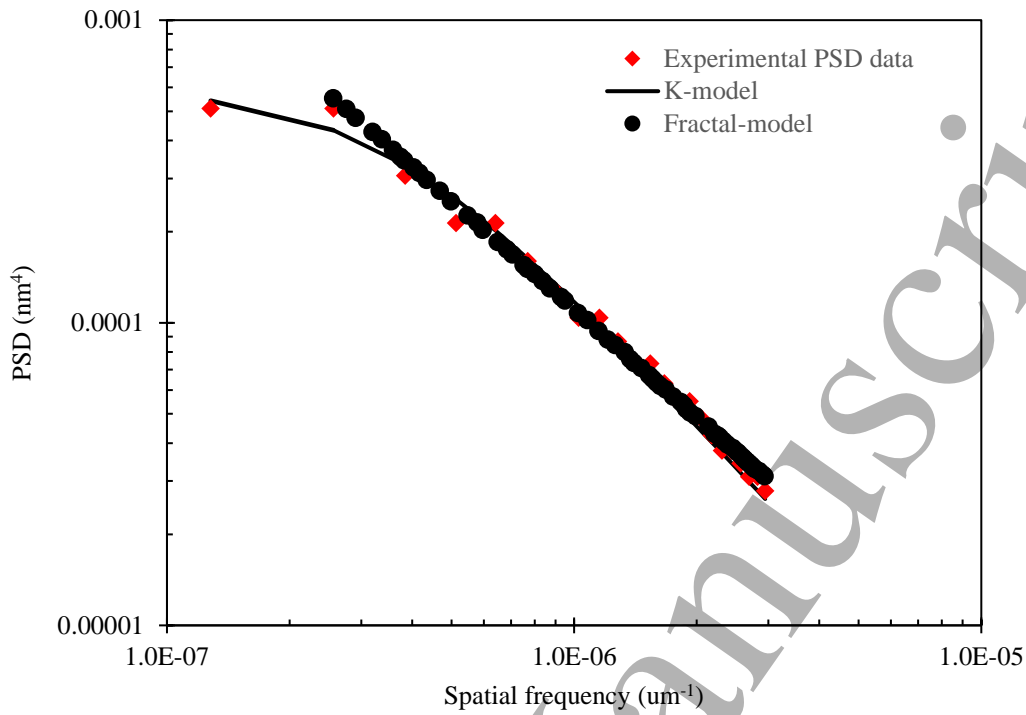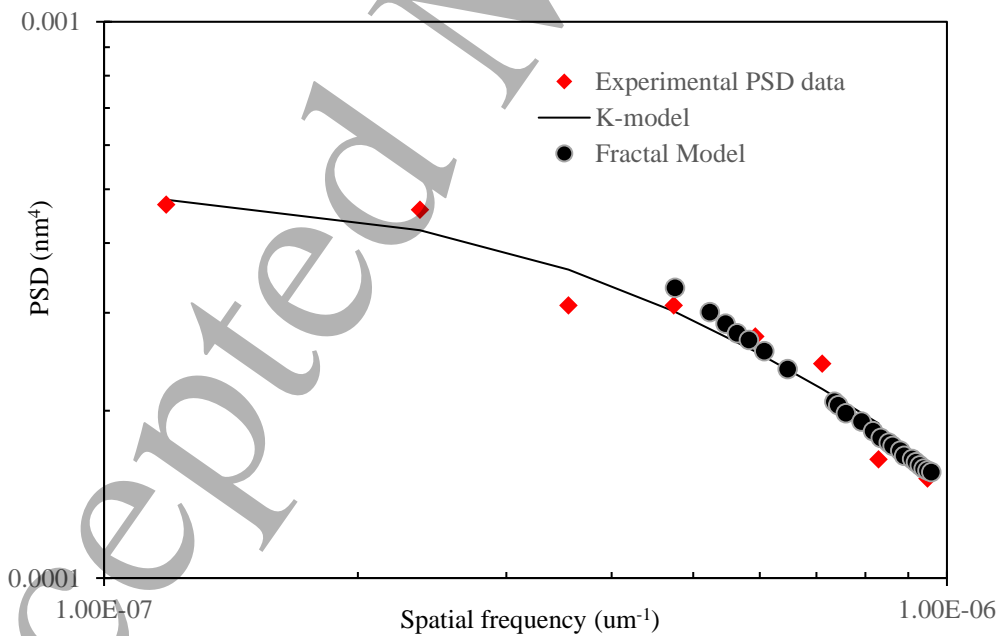
Figure 7. Line profile analysis for the surfaces of Al thin films deposited on mild steel substrates at 200 W

(a)

(b)

Figure 8. PSD profiles displayed on double log scale as functions of spatial frequency for Al thin films deposited on mild steel substrates at (a) 150 W and (b) 200 W. The K-model fits the experimental PSD data at low frequencies whereas the fractal model fits the data at higher spatial frequencies. The model parameters are presented in Table 2.

Table 1 Surface roughness characteristics

Parameters	Stainless Steel Substrate		Mild Steel Substrate	
	150	200	150	200
R_{rms}	30.718 ± 4.02 nm	48.23 ± 26.18 nm	27.59 ± 6.84 nm	38.34 ± 14.62 nm
R_a	23.07 ± 1.05 nm	37.84 ± 22.98 nm	21.86 ± 5.63 nm	29.90 ± 12.02 nm
R_{sk}	0.1976 ± 0.002	-0.703 ± 0.27	-0.168 ± 0.24	-0.015 ± 0.75
R_{ka}	1.153 ± 0.006	5.07 ± 1.73	2.984 ± 0.14	5.94 ± 0.02
H_{av}	29.56 ± 23.88 nm	41.19 ± 8.49 nm	50.44 ± 12.45 nm	96.09 ± 64.44 nm
H_{max}	83.9 nm	96.5 nm	150.4 nm	389 nm
W_{av}	143.88 ± 72.37 nm	135.3 ± 8.674 nm	162.4 ± 10.91 nm	259.70 ± 170.2 nm
W_{max}	540 nm	417 nm	557 nm	903 nm

Table 2 Power Spectral Density Model parameters

Parameters	Stainless Steel Substrate		Mild Steel Substrate	
	150	200	150	200
A	$48 \times 10^3\ nm^3$	$98.5 \times 10^3\ nm^3$	$14.35 \times 10^3\ nm^3$	$14.258 \times 10^3\ nm^3$
B	96 nm	53 nm	346.4 nm	404.5 nm
C	6.71	4.24	0.41	0.38
γ	2.26	2.34	2.18	2.11
K	1.75×10^{-12}	5.88×10^{-14}	8.909×10^{-12}	3.4×10^{-11}
D	2.87	2.83	2.91	2.95
H	0.13	0.17	0.09	0.05
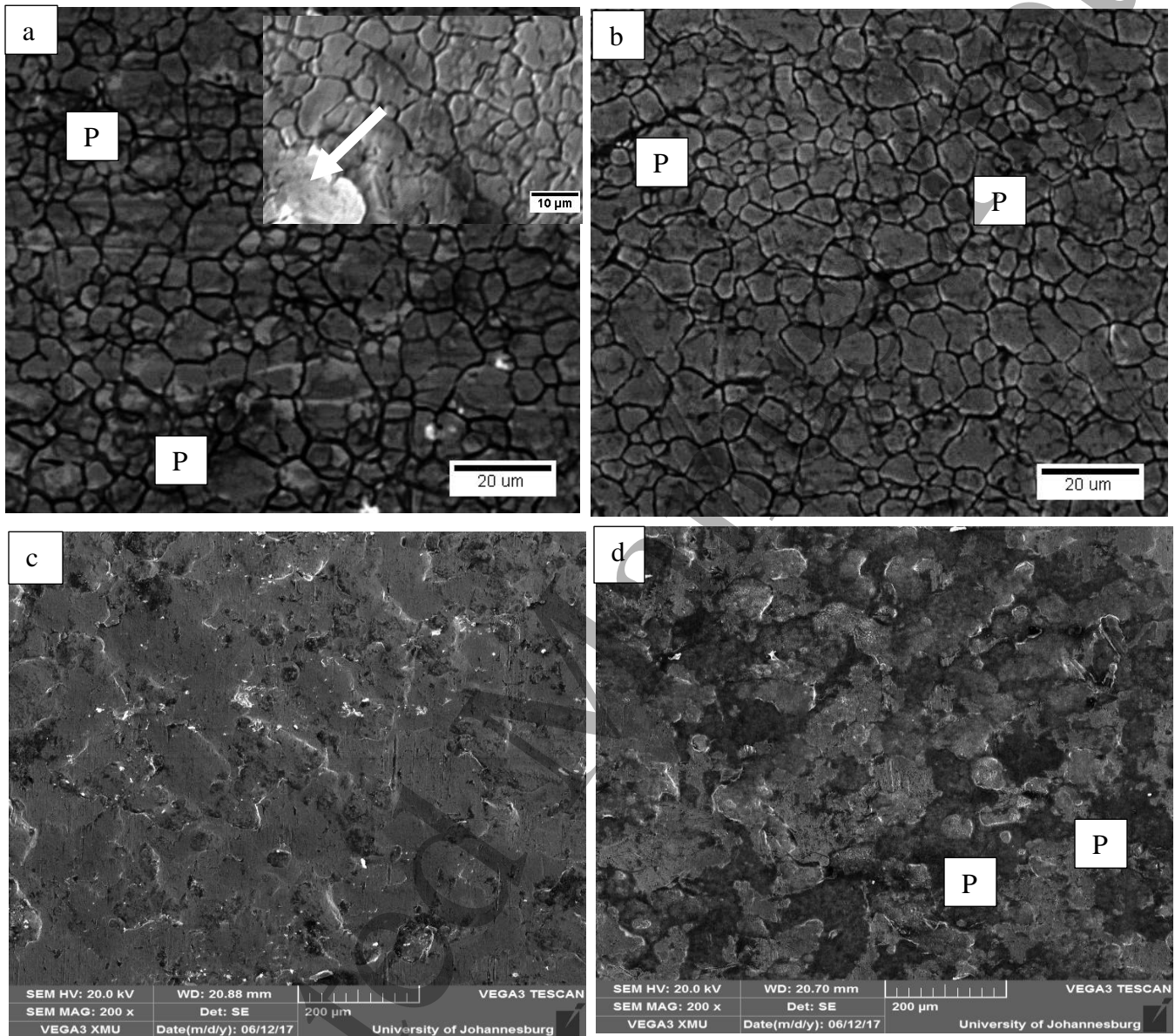
Figure 9. SEM images of Al thin film surfaces deposited on stainless steel substrates at a) 150 W and b) 200 W and mild steel substrate at c) 150 W and d) 200 W. The white arrow in Figure 11a shows the impinged Al structures on the substrate. P indicates dark and highly oxidised porous regions of the microstructures

Figure 10. X-ray diffraction patterns for Al thin films deposited on 316L stainless steel substrate at rf power of (a) 150 W and (b) 200 W

Figure 11. X-ray diffraction patterns for Al thin films deposited on mild steel substrate at rf power of (a) 150 W and (b) 200 W

Acknowledgements

References

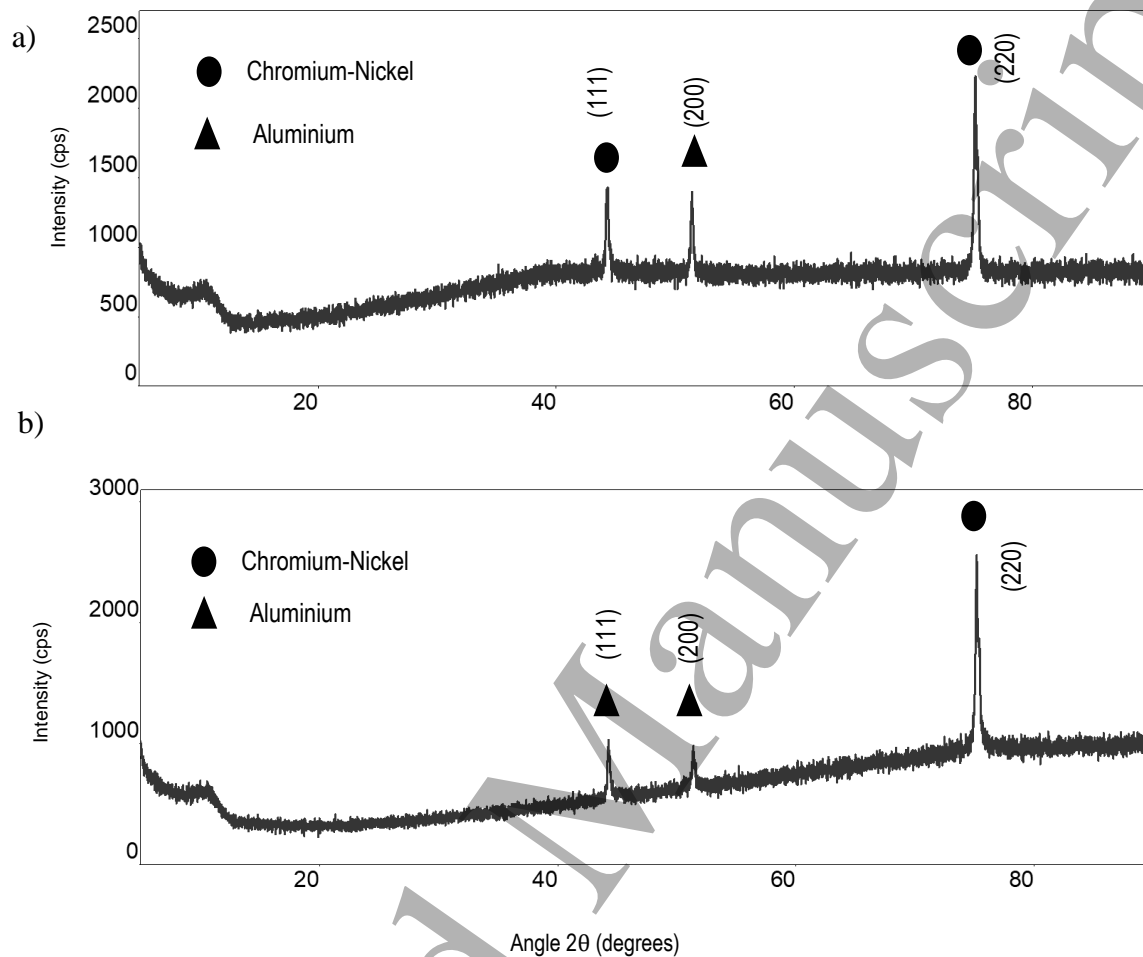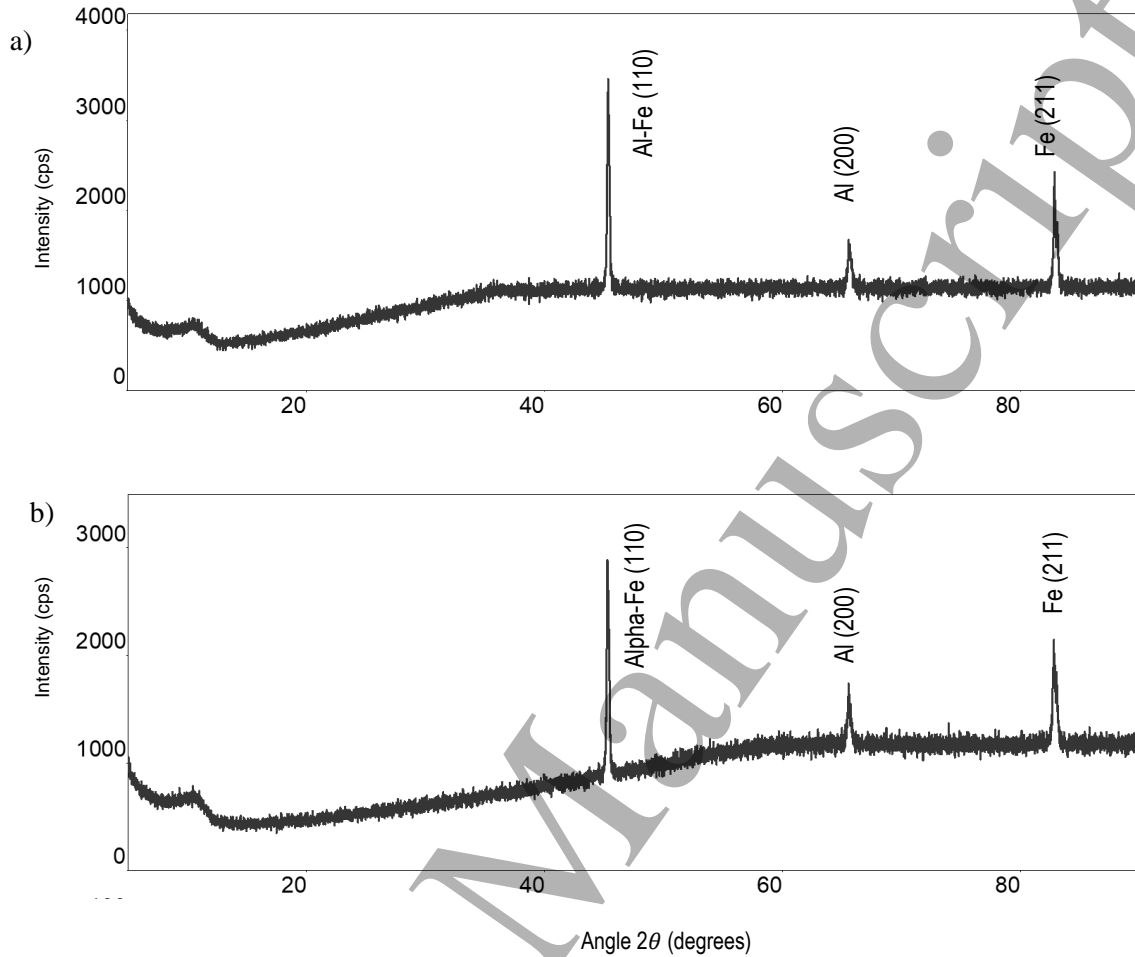[1]   D. Chaliampalias, G. Vourlias, E. Pavlidou, G. Stergioudis, S. Skolianos, and K. Chrissafis, "High temperature oxidation and corrosion in marine environments of thermal spray deposited coatings," *Appl. Surf. Sci.*, vol. 255, no. 5 Part 2, pp. 3104–3111, 2008.

[2]   E. Abedi Esfahani, H. Salimijazi, M. A. Golozar, J. Mostaghimi, and L. Pershin, "Study of corrosion behavior of Arc sprayed aluminum coating on mild steel," *J. Therm. Spray Technol.*, vol. 21, no. 6, pp. 1195–1202, 2012.

[3]   L. M. Liu, Z. Wang, and G. Song, "Study on corrosion resistance properties of hydrothermal sealed arc sprayed aluminium coating," *Surf. Eng.*, vol. 26, no. 6, pp. 399–406, 2010.

[4]   H.-S. Lee, J. Singh, M. Ismail, and C. Bhattacharya, "Corrosion Resistance Properties of Aluminum Coating Applied by Arc Thermal Metal Spray in SAE J2334 Solution with Exposure Periods," *Metals (Basel).*, vol. 6, no. 3, p. 55, 2016.

[5]   R. R. M. H. Pombo, R. S. C. Paredes, S. H. Wido, and A. Calixto, "Comparison of aluminum coatings deposited by flame spray and by electric arc spray," *Surf. Coatings Technol.*, vol. 202, no. 1, pp. 172–179, 2007.

[6]   Z. Panossian *et al.*, "Steel cathodic protection afforded by zinc, aluminium and zinc/aluminium alloy coatings in the atmosphere," *Surf. Coatings Technol.*, vol. 190, no. 2–3, pp. 244–248, 2005.

[7]   D. Dzhurinskiy, E. Maeva, E. Leshchinsky, and R. G. Maev, "Corrosion protection of light alloys using low pressure cold spray," *J. Therm. Spray Technol.*, vol. 21, no. 2, pp. 304–313, 2012.

[8]   A. Pardo *et al.*, "Corrosion protection of Mg/Al alloys by thermal sprayed aluminium coatings," *Appl. Surf. Sci.*, vol. 255, no. 15, pp. 6968–6977, 2009.

[9]   M. S. Han, Y. Bin Woo, S. C. Ko, Y. J. Jeong, S. K. Jang, and S. J. Kim, "Effects of thickness of Al thermal spray coating for STS 304," *Trans. Nonferrous Met. Soc. China*, vol. 19, no. 4, pp. 925–929, 2009.

[10]   H. Garbacz, P. Wieciński, B. Adamczyk-Cieślak, J. Mizera, and K. J. Kurzydłowski, "Studies of aluminium coatings deposited by vacuum evaporation and magnetron sputtering," *J. Microsc.*, vol. 237, no. 3, pp. 475–480, 2010.

[11] E. Wallin, "Alumina Thin Films: From Computer Calculations to Cutting Tools," Linkoping University, Institute of Technology, 2008.

[12] M. Z. Pakhuruddin, K. Ibrahim, and A. A. Aziz, "Properties of Thin aluminium Films on Polyethylene Terephthalate Substrates as Back Contacts in Thin Film Silicon Solar Cells," *Int. J. Polym. Mater.*, vol. 61, no. 9, pp. 669–678, 2012.

[13] S. Kuroda, J. Kawakita, and M. Takemoto, "An 18-year exposure test of thermal-sprayed Zn, Al, and Zn-Al coatings in marine environment," *Corrosion*, vol. 62, no. 7, pp. 635–647, 2006.

[14] F. M. D'Heurle, "Aluminum films deposited by rf sputtering," *Metall. Mater. Trans. B*, vol. 1, no. 3, pp. 725–732, 1970.

[15] D. V Sidelev, A. V Yuryeva, V. P. Krivobokov, A. S. Shabunin, M. S. Syrtanov, and Z. Koishybayeva, "Aluminum films deposition by magnetron sputtering systems: Influence of target state and pulsing unit," *J. Phys. Conf. Ser.*, vol. 741, no. 1, p. 12193, 2016.

[16] M. T. Kao and J. F. Lin, "Effects of deposition conditions of the Al film in Al/glass specimens and annealing conditions on internal stresses and hillock formations," *Thin Solid Films*, vol. 520, no. 16, pp. 5353–5360, 2012.

[17] S. Kim, H. . Choi, and S. . Choi, "A study on the crystallographic orientation with residual stress and electrical property of Al films deposited by sputtering," *Thin Solid Films*, vol. 322, no. 1–2, pp. 298–302, 1998.

[18] G. P. Panta and D. P. Subedi, "Electrical Characterization of Aluminum (Al) Thin Films Measured By Using Four-Point Probe Method," *Kathmandu Univ. J. Sci. Eng. Technol.*, vol. 8, no. II, pp. 31–36, 2012.

[19] S. J. Hwang, J. H. Lee, C. O. Jeong, and Y. C. Joo, "Effect of film thickness and annealing temperature on hillock distributions in pure Al films," *Scr. Mater.*, vol. 56, no. 1, pp. 17–20, 2007.

[20] C. C. Peng, C. K. Chung, and J. F. Lin, "Effects of Al film thickness and annealing temperature on the aluminum-induced crystallization of amorphous silicon and carrier mobility," *Acta Mater.*, vol. 59, no. 15, pp. 6093–6102, 2011.

[21] I. Petrov, P. B. Barna, L. Hultman, and J. E. Greene, "Microstructural evolution during film growth," *J. Vac. Sci. Technol. A*, vol. 21, p. S117, 2003.

[22] M. F. Erinosho and E. T. Akinlabi, "Estimation of Surface Topography and Wear Loss of Laser Metal-Deposited Ti6Al4V and Cu," *Adv. Eng. Mater.*, vol. 18, no. 8, pp. 1396–1405, 2016.

[23] K. L. Westra and D. J. Thomson, "The microstructure of thin films observed using atomic force microscopy," *Thin Solid Films*, vol. 257, no. 1. pp. 15–21, 1995.

[24] S. H. Davies, B. Karnik, M. J. Baumann, and S. Masten, "AFM and SEM characterization of iron oxide coated ceramic membranes," *J. Mater. Sci.*, vol. 41, pp. 6861–6870, 2006.

[25] M. Kwoka, L. Ottaviano, and J. Szuber, "AFM study of the surface morphology of L-CVD

SnO 2 thin films," *Thin Solid Films*, vol. 515. pp. 8328–8331, 2007.

[26] Z. N. Fang, B. Yang, M. G. Chen, C. H. Zhang, J. P. Xie, and G. X. Ye, "Growth and morphology of ultra-thin Al films on liquid substrates studied by atomic force microscopy," *Thin Solid Films*, vol. 517, no. 11. pp. 3408–3411, 2009.

[27] J. Xie, X. Lu, Y. U. Zhu, C. Liu, and N. Bao, "Atomic force microscopy (AFM) study on potassium hexatitanate whisker (K 2 O · 6TiO 2)," *J. Mater. Sci.*, vol. 8, pp. 3641–3646, 2003.

[28] M. Cremona *et al.*, "Grain size distribution analysis in polycrystalline LiF thin films by mathematical morphology techniques on AFM images and X-ray diffraction data," *J. Microsc.*, vol. 197, no. 3, pp. 260–267, 2000.

[29] Y. Gong, S. T. Misture, P. Gao, and N. P. Mellott, "Surface Roughness Measurements Using Power Spectrum Density Analysis with Enhanced Spatial Correlation Length," *J. Phys. Chem. C*, vol. 120, no. 39, pp. 22358–22364, 2016.

[30] M. Aqil, M. Azam, M. Aziz, and R. Latif, "Deposition and Characterization of Molybdenum Thin Film Using Direct Current Magnetron and Atomic Force Microscopy," *J. Nanotechnol.*, vol. 2017, pp. 1–10, 2017.

[31] M. Senthilkumar, N. K. Sahoo, S. Thakur, and R. B. Tokas, "Characterization of microroughness parameters in gadolinium oxide thin films: A study based on extended power spectral density analyses," *Appl. Surf. Sci.*, vol. 252, no. 5, pp. 1608–1619, 2005.

[32] D. Aurongzeb, "Growth instability and surface phase transition of Ti thin film on Si(111): An Atomic force microscopy study," *Appl. Surf. Sci.*, vol. 252, pp. 6135–6140, 2006.

[33] N. Muslim, Y. W. Soon, C. M. Lim, and N. Y. Voo, "Influence of Sputtering Power on Properties of Titanium Thin Films Deposited By Rf Magnetron Sputtering," *ARPN J. Eng. Appl. Sci.*, vol. 10, no. 16, pp. 7184–7189, 2015.

[34] N. G. Semaltianos, "Thermally evaporated thin aluminium films," *Appl. Surf. Sci.*, vol. 183, no. 3–4, pp. 223–229, 2001.

[35] C. Xu, H. Tian, C. E. Reece, and M. J. Kelley, "Topographic power spectral density study of the effect of surface treatment processes on niobium for superconducting radio frequency accelerator cavities," *Phys. Rev. Spec. Top. - Accel. Beams*, vol. 15, no. 4, 2012.

[36] R. Gavrila, A. Dinescu, and D. Mardare, "A Power Spectral Density Study of Thin Films Morphology Based on AFM Profiling," *Rom. J. Inf. Sci. Technol.*, vol. 10, no. 3, pp. 291–300, 2007.

[37] A.A. Ponomareva, V. a Moshnikov, and G. Suchaneck, "Microstructural Characterization of Hierarchical Structured Surfaces by Atomic Force Microscopy," *IOP Conf. Ser. Mater. Sci. Eng.*, vol. 47, p. 12052, 2013.

[38] S. Srivastav, S. Dhillon, R. Kumar, and R. Kant, "Experimental validation of roughness power spectrum-based theory of anomalous cottrell response," *J. Phys. Chem. C*, vol. 117, no. 17, pp. 8594–8603, 2013.

[39] A. V. Novak and V. R. Novak, "Roughness of amorphous, polycrystalline and hemispherical-grained silicon films," *Tech. Phys. Lett.*, vol. 39, no. 10, pp. 858–861, 2013.

[40] C.-M. Chiang and L.-S. Chang, "Microstructure and characterization of aluminum oxide thin films prepared by reactive RF magnetron sputtering on copper," *Surf. Coatings Technol.*, vol. 198, no. 1–3, pp. 152–155, 2005.

[41] K. Bordo and H. G. Rubahn, "Effect of deposition rate on structure and surface morphology of thin evaporated al films on Dielectrics and Semiconductors," *Medziagotyra*, vol. 18, no. 4, pp. 313–317, 2012.

[42] F.M. Mwema, O.P. Oldijo, S.A. Akinlabi and E. T. Akinlabi, "Properties of physically deposited thin aluminium film coatings: A review," *Journal of alloys and compounds*, vol. 747, pp. 306–323, 2018.

[43] C. Musaoglu, P. Pat, S. Ozen and S. Korkmaz, "Investigation of the structural, surface, optical and electrical properties of the Indium 2 doped Cu_xO thin films deposited by a thermionic vacuum arc" *Material Research Express in Press*, 2018.

[44] N. Liu and Y. Liu, "Suppressing Hillock Formation in Si-supported Pure Al Films" *Material Research Express in Press*, 2018.

[45] T. D. B. Jacobs, T. Junge, and L. Pastewka, "Quantitative characterization of surface topography using spectral analysis," *Surf. Topogr. Metrol. Prop.*, vol. 5, no. 1, p. 13001, 2017